**THE EUROPEAN
PHYSICAL JOURNAL B**

Regular Article

Bifurcation and resonance in a fractional Mathieu-Duffing oscillator

J.H. Yang[1,2,a], Miguel A.F. Sanjuán[3], and H.G. Liu[1]

[1] School of Mechatronic Engineering, China University of Mining and Technology, Xuzhou 221116, P.R. China
[2] Jiangsu Key Laboratory of Mine Mechanical and Electrical Equipment, China University of Mining and Technology, Xuzhou 221116, P.R. China
[3] Nonlinear Dynamics, Chaos and Complex Systems Group, Departamento de Física, Universidad Rey Juan Carlos, Tulipán s/n, 28933 Móstoles, Madrid, Spain

Abstract. The bifurcation and resonance phenomena are investigated in a fractional Mathieu-Duffing oscillator which contains a fast parametric excitation and a slow external excitation. We extend the method of direct partition of motions to evaluate the response for the parametrically excited system. Besides, we propose a numerical method to simulate different types of local bifurcation of the equilibria. For the nonlinear dynamical behaviors of the considered system, the linear stiffness coefficient is a key factor which influences the resonance phenomenon directly. Moreover, the fractional-order damping brings some new results that are different from the corresponding results in the ordinary Mathieu-Duffing oscillator. Especially, the resonance pattern, the resonance frequency and the resonance magnitude depend on the value of the fractional-order closely.

1 Introduction

Parametric excitations are used in the mathematical modeling of different phenomena in many scientific and engineering fields [1–6]. If there is resonance phenomenon in the response, the structure of the system may be destroyed and then might lead to a disaster. Hence, it is important to investigate the resonance phenomena in parametrically excited systems. There are lots of references focusing on this topic. Furthermore, parametric excitations usually exist in a high-frequency form [7–13]. Moreover, besides the fast parametric excitation, there may be other slow excitation acting on a physical or mechanical structure. Although the slow excitation is often in a weak strength, it usually indicates the characteristic information in some occasions. This makes the researchers to be interested in the response induced by a slow excitation. In a nonlinear system, if the fast and slow excitations are both external and act on a nonlinear system simultaneously, the response of the system to the weak slow excitation can be enhanced by the fast excitation. This is precisely what happens with the well-known vibrational resonance phenomenon [14]. The vibrational resonance phenomenon exists in many systems [15–20]. However, if the system is excited by a fast parametric excitation and a slow external excitation, the response to the low-frequency excitation is a noteworthy problem. Certainly,

there is less work done on this topic, and this is one of our motivations.

In the present work, we consider the Mathieu-Duffing oscillator which is a typical parametrically excited system. The excitations include a slow external excitation and a fast parametric excitation. Without loss of generality, we let the damping in the fractional-order form. The fractional-order damping is widely used in many disciplines, especially in rheology [21,22], viscoelasticity [23,24], quantum systems [25–27], mechanics [28,29], electrochemistry [30,31], bioengineering [32], automatic control [33], etc., just to cite a few. The fractional-order damping influences the bifurcation and resonance behaviors in the nonlinear system that are subjected to both fast and slow excitations [34–37]. We concentrate our study on the dynamical behavior of the fractional Mathieu-Duffing oscillator.

The outline of the paper is organized as follows. In Section 2, we obtain the magnitude of the constant component and the response amplitude to the low-frequency excitation in the response. In Section 3, we give a numerical method to verify the local bifurcation of the equilibria. In Section 4, the parameter induced resonance and the resonance frequency is investigated thoroughly. The effects of the system parameter and the fractional-order damping on the resonance are discussed in detail. In Section 5, we conclude the main results of this paper.

a e-mail: jianhuayang@cumt.edu.cn

2 Theoretical framework

The fractional Mathieu-Duffing oscillator is governed by the equation

$$\frac{d^2 x}{dt^2} + \delta \frac{d^\alpha x}{dt^\alpha} + [a + F \cos(\Omega t)] x + bx^3 = f \cos(\omega t). \quad (1)$$

In equation (1), $\delta > 0$ is the damping coefficient. The operator $\frac{d^\alpha x}{dt^\alpha}$ denotes the fractional-order damping. The value of the fractional-order α usually lies in the interval $(0, 2)$. There are three algorithms widely used for the fractional-order differential operator, i.e., the Caputo algorithm, the Grünwald-Letnikov algorithm, and the Riemann-Liouville algorithm [38]. In equation (1), we adopt the Grünwald-Letnikov algorithm which is given by the formula

$$\left. \frac{d^\alpha f(t)}{dt^\alpha} \right|_{t=kh} = \lim_{h \to 0} \frac{1}{h^\alpha} \sum_{j=0}^{k} (-1)^j \binom{\alpha}{j} f(kh - jh), \quad (2)$$

where the binominal coefficient is

$$\binom{\alpha}{j} = \frac{\Gamma(\alpha + 1)}{\Gamma(j + 1)\Gamma(\alpha - j + 1)}. \quad (3)$$

In the system, the parameters a and b are the linear and nonlinear stiffness coefficient, respectively. Ignoring the parametric excitation, the system is a Duffing oscillator with a double-well potential when $a < 0$ and $b > 0$, while it has a single-well potential when $a > 0$ and $b > 0$, and it has a double-hump well when $a > 0$ and $b < 0$. The frequencies of the harmonic excitations satisfy $\omega \ll \Omega$. The amplitude F has the same magnitude order as the linear stiffness a. The amplitude f is small, $f \ll 1$.

According to the method of direct partition of slow and fast motions [39,40], we let the approximated solution of equation (1) in the form $x = X + \Psi$, where X and Ψ are slow and fast motions with period $2\pi/\omega$ and $2\pi/\Omega$, respectively. Then, equation (1) turns to

$$\frac{d^2 X}{dt^2} + \frac{d^2 \Psi}{dt^2} + \delta \frac{d^\alpha X}{dt^\alpha} + \delta \frac{d^\alpha \Psi}{dt^\alpha}$$
$$+ aX + a\Psi + bX^3 + 3bX^2\Psi + 3bX\Psi^2 + b\Psi^3$$
$$= -XF \cos(\Omega t) - \Psi F \cos(\Omega t) + f \cos(\omega t). \quad (4)$$

We seek the approximate solution of Ψ in the linear equation

$$\frac{d^2 \Psi}{dt^2} + \delta \frac{d^\alpha \Psi}{dt^\alpha} + a\Psi = -XF \cos(\Omega t). \quad (5)$$

It is easy to obtain $\Psi = A_H \cos(\Omega t - \theta_H)$, where

$$\begin{cases} A_H = \frac{XF}{\sqrt{\left(a - \Omega^2 + \delta\Omega^\alpha \cos\frac{\alpha\pi}{2}\right)^2 + \left(\delta\Omega^\alpha \sin\frac{\alpha\pi}{2}\right)^2}}, \\ \theta_H = -\tan^{-1}\frac{\delta\Omega^\alpha \sin\frac{\alpha\pi}{2}}{a - \Omega^2 + \delta\Omega^\alpha \cos\frac{\alpha\pi}{2}}. \end{cases} \quad (6)$$

Here, the amplitude of the fast variable is related to the slow variable. It is different from the corresponding results when the two excitations act as external perturbations.

Substituting the solution of Ψ into equation (4) and averaging all terms in the range $[0, 2\pi/\Omega]$, we obtain that the equation for the slow variable is:

$$\frac{d^2 X}{dt^2} + \delta \frac{d^\alpha X}{dt^\alpha} + \left(a + \frac{F^2 \cos\theta_H}{2\mu}\right) X$$
$$+ b\left(1 + \frac{3F^2}{2\mu^2}\right) X^3 = f \cos(\omega t), \quad (7)$$

where

$$\mu = \sqrt{\left(a - \Omega^2 + \delta\Omega^\alpha \cos\frac{\alpha\pi}{2}\right)^2 + \left(\delta\Omega^\alpha \sin\frac{\alpha\pi}{2}\right)^2}.$$

From equation (7), we find that the fast excitation and the fractional-order influence both the linear and the nonlinear stiffness. It is very different from the results when the fast excitation is not a parametric but an external excitation. In that case, the fast excitation and the fractional-order influence the linear stiffness coefficient a only, as mentioned in the previous articles [34,36,37,41]. The pitchfork bifurcation will occur when the local stability of the equilibria of the equivalent system described in equation (7) changes. On the one hand, if the parameter b is positive, the term $b(1 + \frac{3F^2}{2\mu^2})$ is also positive. For the case $a > 0$, we also have $a + \frac{F^2 \cos\theta_H}{2\mu} > 0$ and there is no pitchfork bifurcation. For the case $a < 0$, the term $a + \frac{F^2 \cos\theta_H}{2\mu}$ may change its sign with the change of the fractional-order α. It may lead to a pitchfork bifurcation. If $a + \frac{F^2 \cos\theta_H}{2\mu} \geq 0$, the equivalent system in equation (7) has one stable equilibrium $X^* = 0$ only. Else, equation (7) has one unstable equilibrium $X^* = 0$ and two stable equilibria

$$X^* = \pm\sqrt{-\frac{2a\mu^2 + \mu F^2 \cos\theta_H}{b(2\mu^2 + 3F^2)}}.$$

On the other hand, if the parameter b is negative, the term $b(1 + \frac{3F^2}{2\mu^2})$ is also negative. Equation (7) has only one stable equilibrium $X^* = 0$ for the case $a + \frac{F^2 \cos\theta_H}{2\mu} > 0$. Or else, equation (7) has no stable equilibrium and the system will diverge to infinity for the case $a + \frac{F^2 \cos\theta_H}{2\mu} \leq 0$.

To obtain the linear response of the system to the slow excitation, we let $X = y + y_0$. Here, y is a harmonic component with frequency ω and y_0 is the constant component in the response. We assume y_0 just equals the value of the stable equilibria X^*. Hence, for the case $b > 0$,

$$y_0 = X^* = \begin{cases} 0, & a + \frac{F^2 \cos\theta_H}{2\mu} \geq 0, \\ \pm\sqrt{-\frac{2a\mu^2 + \mu F^2 \cos\theta_H}{b(2\mu^2 + 3F^2)}}, & a + \frac{F^2 \cos\theta_H}{2\mu} < 0. \end{cases} \quad (8)$$

For the case $b < 0$,

$$y_0 = X^* = \begin{cases} 0, & a + \frac{F^2 \cos\theta_H}{2\mu} > 0, \\ null, & a + \frac{F^2 \cos\theta_H}{2\mu} \leq 0. \end{cases} \quad (9)$$

This assumption will be verified in the following section. Then, equation (7) turns to:

$$\frac{d^2y}{dt^2} + \delta\frac{d^\alpha y}{dt^\alpha} + \omega_r y + 3\beta X^* y^2 + \beta y^3 = f\cos(\omega t), \quad (10)$$

where $\omega_r = a + \frac{F^2\cos\theta_H}{2\mu} + 3\beta X^{*2}$ and $\beta = b(1 + \frac{3F^2}{2\mu^2})$. Seeking the approximate solution of y in the linear equation

$$\frac{d^2y}{dt^2} + \delta\frac{d^\alpha y}{dt^\alpha} + \omega_r y = f\cos(\omega t). \quad (11)$$

One gets $y = A_L\cos(\omega t - \theta_L)$, where

$$\begin{cases} A_L = \frac{f}{\sqrt{\left(\omega_r - \omega^2 + \delta\omega^\alpha\cos\frac{\alpha\pi}{2}\right)^2 + \left(\delta\omega^\alpha\sin\frac{\alpha\pi}{2}\right)^2}}, \\ \theta_L = \tan^{-1}\frac{\delta\omega^\alpha\sin\frac{\alpha\pi}{2}}{\omega_r - \omega^2 + \delta\omega^\alpha\cos\frac{\alpha\pi}{2}}. \end{cases} \quad (12)$$

To quantify the resonance character of the system, a target named response amplitude and labeled by Q will be used, $Q = A_L/f$. From equation (12), we have

$$Q = \frac{1}{\sqrt{\left(\omega_r - \omega^2 + \delta\omega^\alpha\cos\frac{\alpha\pi}{2}\right)^2 + \left(\delta\omega^\alpha\sin\frac{\alpha\pi}{2}\right)^2}}. \quad (13)$$

The resonance behavior can be predicted by the result in equation (13).

3 The local bifurcation of the equilibria

In last section, we assume that the constant component in the response equals the value of the stable equilibrium of the equivalent system. Certainly, this assumption needs to be verified. In the previous literatures, this assumption usually has been verified by some phase diagrams for some control parameters [42–44]. Through the phase diagrams, it can be found that the phase portraits revolve around the stable equilibrium of the equivalent system. However, this is an imperfect method. On the one hand, the constant component in the response cannot be read directly. On the other hand, the phase diagram is given only for some special parameters. However, we need to know the change tendency of the constant component in the response when the control parameter changes continuously. Hence, we need to extract the constant component directly from the time series of equation (1).

There are some method to discretize the factional-order operator [45–50]. In the following numerical calculation, we adopt the definition of the Grünwald-Letnikov algorithm to discretize the equation for its simplicity [34,38,50]. For numerically computing the constant component from the time series, the Fourier series is a useful tool. If we have one absolutely integrable function $f(x)$ in the interval $[0, 2\pi]$, its Fourier expansion is in the form

$$f(x) = \frac{a_0}{2} + \sum_{n=1}^{\infty}(a_n\cos nx + b_n\sin nx), \quad (14)$$

where the cosine and sine Fourier coefficients are

$$\begin{cases} a_n = \frac{1}{\pi}\int_0^{2\pi} f(x)\cos(nx)dx & (n = 0, 1, 2, \ldots) \\ b_n = \frac{1}{\pi}\int_0^{2\pi} f(x)\sin(nx)dx & (n = 1, 2, \ldots). \end{cases} \quad (15)$$

From equation (15), we have that the coefficient a_0 is

$$a_0 = \frac{1}{\pi}\int_0^{2\pi} f(x)dx. \quad (16)$$

To obtain more accurate results, for the numerical simulation of a_0 from the time series $x(t)$, it should be calculated by the following equation, i.e.,

$$a_0 = \frac{2}{rT}\int_0^{rT} x(t)dt, \quad (17)$$

where $T = 2\pi/\omega$ and r is a large integer number. From the Fourier expansion in equation (14), we know that the constant component in the time series should be $\frac{a_0}{2}$ but not a_0. Hence, for the numerical simulation, the constant component in the response should be computed by

$$y_0 = X^* = \frac{1}{rT}\int_0^{rT} x(t)dt. \quad (18)$$

In Figure 1, for different values of the fractional-order α, the constant component in the response are plotted according to the analytical prediction in equation (8) and the numerical simulation formula in equation (18), respectively. It is found that the numerical results are in good agreement with the analytical predictions. An important fact is that the bifurcation behavior occurs in the diagram. Approaching to the value $a = 0$, the pitchfork bifurcation occurs. This type of bifurcation also appears when the two excitations are both external. From Figure 1, we find that this local bifurcation also occurs when the excitations act in a parametric and external way. Through Figure 1, we verify the assumption that the constant component in the response just equals to the value of the stable equilibrium of the equivalent system. Hence, this method can be used to verify the local bifurcation of the equilibria. Certainly, besides the pitchfork bifurcation, this numerical method can also be used to verify other types of local bifurcation, such as the saddle-node bifurcation and the transcritical bifurcation.

4 Resonance analysis

For the numerical simulation, Q can be obtained directly from the time series of $x(t)$. According to the definition of Q and the Fourier coefficient in equation (14) and equation (15), Q should be computed by the formula

$$Q(\omega) = \sqrt{Q_{\sin}^2(\omega) + Q_{\cos}^2(\omega)}/f, \quad (19)$$

where

$$Q_{\sin}(\omega) = \frac{2}{rT}\int_0^{rT} x(t)\sin(\omega t)dt,$$

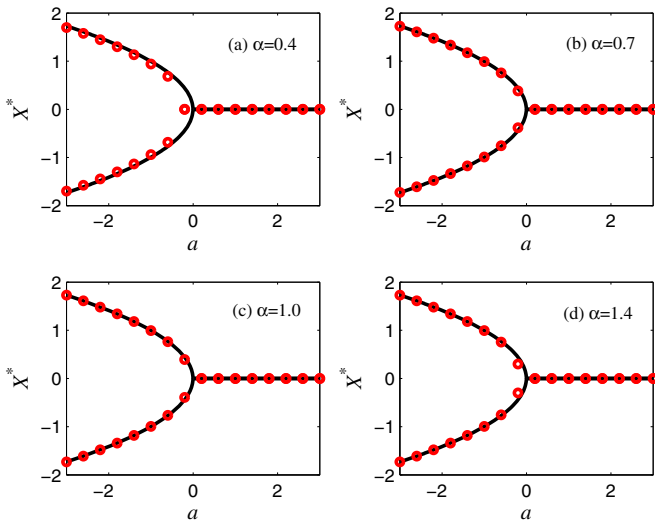$$Q_{\cos}(\omega) = \frac{2}{rT}\int_0^{rT} x(t)\cos(\omega t)dt. \quad (20)$$

Fig. 1. The pitchfork bifurcation is induced by the system parameter a for different fractional-order values. The continuous lines are plotted by the analytical method and the discrete points are plotted by the numerical method. The simulation parameters are $\delta = 1.2$, $b = 1$, $f = 0.1$, $\omega = 0.5$, $F = 1$, $\Omega = 10$.

We will analyse the parameter induced resonance and the resonance frequency in this section.

4.1 The resonance induced by the system parameter a

For the case $b > 0$, if we make the system parameter a as the control parameter, the three-dimensional curve of the response amplitude Q versus the linear stiffness coefficient a and the fractional-order α are plotted in Figure 2 according to the analytical prediction in equation (13). On the one hand, for a fixed fractional-order α, the response amplitude Q versus the linear stiffness a presents a resonance phenomenon. On the other hand, with the increase of α, the curve of $Q - a$ turns from a single-resonance pattern to a double-resonance pattern. Furthermore, for a fixed a, the magnitude of the resonance peak will turn larger by increasing the fractional-order α. In a word, the linear stiffness coefficient a can induce the resonance phenomenon in the fractional Mathieu-Duffing oscillator.

To reveal the effect of the linear stiffness coefficient a on the resonance phenomenon much more clearly, we plot Figure 3 which shows the $Q - a$ curve on the two-dimensional plane. In this figure, for the case $\alpha = 0.4$ and $\alpha = 0.7$, the curve $Q - a$ is in a single-resonance mode. The resonance occurs near $a = 0$. For the case $\alpha = 1.0$ and $\alpha = 1.4$, the curve $Q - a$ is in the double-resonance mode. Actually, the value $a = 0$ is not the resonance peak location. At the resonance peak, the critical value of a is a little larger or smaller than the zero value. For a larger value of α, the magnitude of the resonance peak of Q is larger too. Especially in Figure 3c, $\alpha = 1$, the original system degenerate to the ordinary Mathieu-Duffing oscillator. Comparing Figure 3c with Figures 3a and 3b,
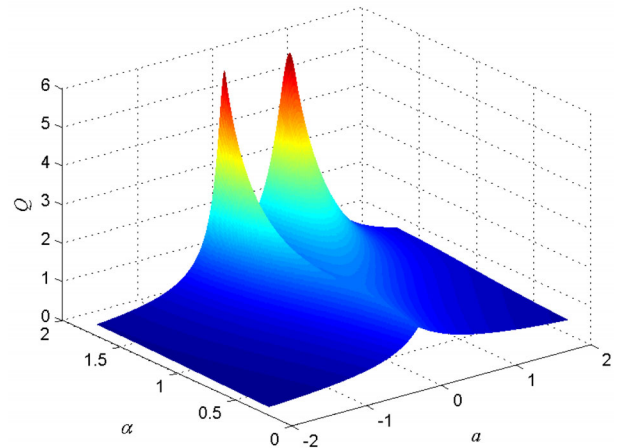

Fig. 2. The analytical result of the response amplitude Q versus the fractional-order α and the linear stiffness coefficient a. The simulation parameters are $\delta = 1.2$, $b = 1$, $f = 0.1$, $\omega = 0.5$, $F = 1$, $\Omega = 10$.
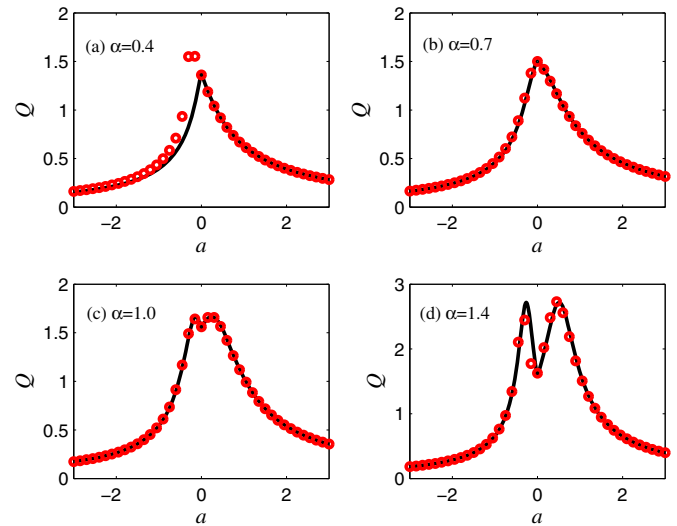

Fig. 3. The resonance is induced by the linear stiffness coefficient a. The continuous lines are the analytical results and the discrete points are the numerical results. The simulation parameters are $\delta = 1.2$, $b = 1$, $f = 0.1$, $\omega = 0.5$, $F = 1$, $\Omega = 10$.

we know that the resonance pattern turns to single resonance when the fractional-order $\alpha < 1$. It indicates that the fractional-order may induce different resonance pattern. Comparing Figure 3c with Figure 3d, we know that the double resonance pattern turns much more apparently when $1 < \alpha < 2$. In this figure, the analytical result of the response amplitude Q is in good agreement with the numerical simulation. It verifies the analytical prediction for the response amplitude Q.

For the case $b < 0$, according to the analytical result in equation (13), the three-dimensional curve of Q versus the linear stiffness coefficient a and the fractional-order α is shown in Figure 4. For a fixed parameter a, the magnitude of the response amplitude increases by increasing α.
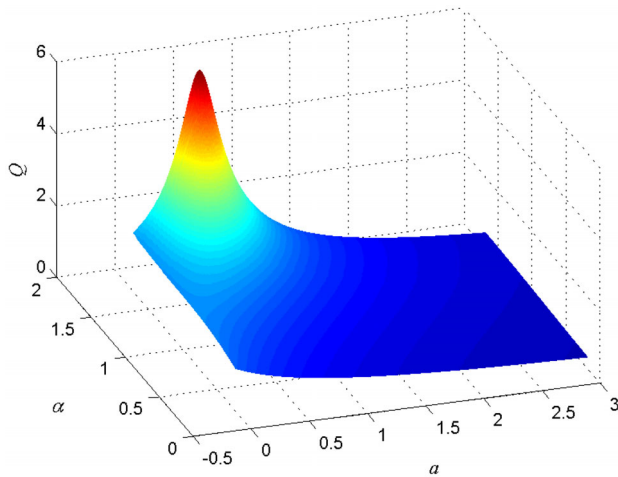
Fig. 4. The analytical result of the response amplitude Q versus the fractional-order α and the linear stiffness coefficient a. The simulation parameters are $\delta = 1.2$, $b = -1$, $f = 0.1$, $\omega = 0.5$, $F = 1$, $\Omega = 10$.
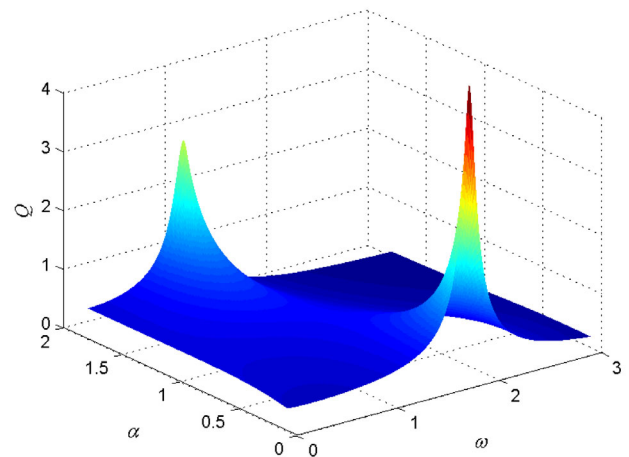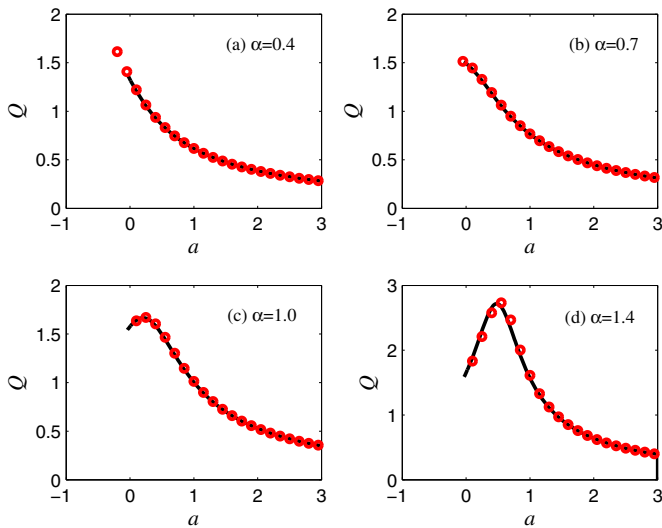

Fig. 6. The analytical result of the response amplitude Q versus the fractional-order α and the low-frequency ω. The simulation parameters are $\delta = 1.2$, $a = -1$, $b = 1$, $f = 0.1$, $F = 1$, $\Omega = 30$.

Fig. 5. The resonance is induced by the linear stiffness coefficient a. The continuous lines are the analytical results and the discrete points are the numerical results. The simulation parameters are $\delta = 1.2$, $b = -1$, $f = 0.1$, $\omega = 0.5$, $F = 1$, $\Omega = 10$.
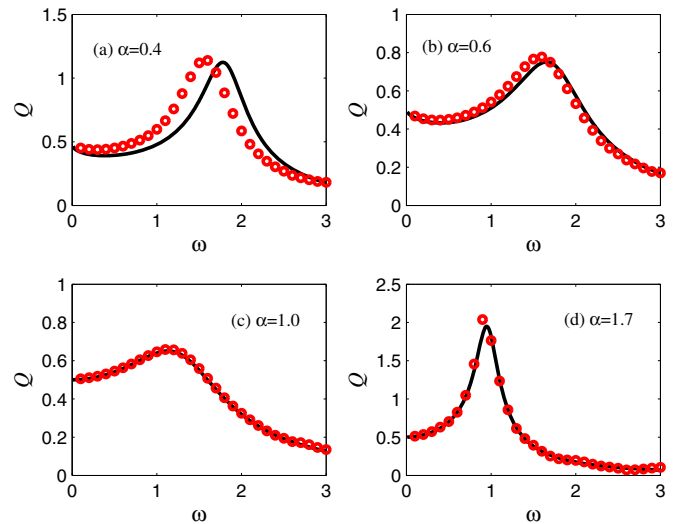

Fig. 7. The resonance frequency is shown for different values of the fractional-order α. The continuous lines are the analytical results and the discrete points are the numerical results. The simulation parameters are $\delta = 1.2$, $a = -1$, $b = 1$, $f = 0.1$, $F = 1$, $\Omega = 30$.

The occurrence of the resonance phenomenon depends on the fractional-order α closely.

In Figure 5, for the case $b < 0$, the curve $Q - a$ is plotted according to analytical and numerical results for different values of α in the two-dimensional plane. In Figures 5a and 5b, by increasing the linear stiffness a, the response amplitude Q will decrease. In Figures 5c and 5d, there is a resonance phenomenon with the variation of a. When $a < 0$, the response amplitude Q does not exist. This is because the response is divergent for this case. Comparing the response of the ordinary Mathieu-Duffing oscillator in Figure 5c with the response of the fractional Mathieu-Duffing oscillator in Figures 5a, 5b and 5d, we find that the value of α influences the resonance pattern

and the magnitude of Q too. It is similar to the results for the case $b > 0$.

4.2 The resonance frequency

The frequency response is important in the engineering field. Through the frequency response curve, we can determine the resonance frequency. For the case $a < 0$ and $b > 0$, the analytical result of Q versus the low-frequency ω and the fractional-order α is plotted in Figure 6. When the fractional-order is far away from the value $\alpha = 1$, the resonance may have a large magnitude.

In Figure 7, the frequency response curve is plotted in the two-dimensional curve. We choose four different values
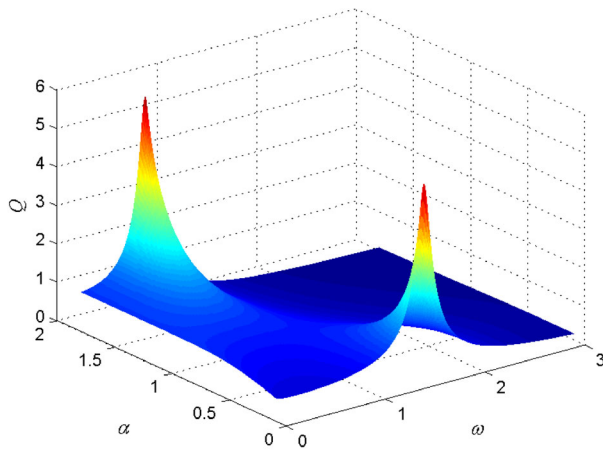
Fig. 8. The analytical result of the response amplitude Q versus the fractional-order α and the low-frequency ω. The simulation parameters are $\delta = 1.2$, $a = 1$, $b = 1$, $f = 0.1$, $F = 1$, $\Omega = 30$.

for the fractional-order α and other simulation parameters are the same with that in Figure 6. In Figure 7, we find that both the resonance frequency and the resonance value depend on the fractional-order α. By increasing the fractional-order α, the resonance frequency turns small. Compared with the frequency response curve of the ordinary Mathieu-Duffing oscillator as shown in Figure 7c, the resonance phenomenon is much stronger in the frequency response curve of the fractional Mathieu-Duffing oscillator as shown in Figures 7a, 7b and 7d.

For the case $a > 0$ and $b > 0$, the frequency response curve versus the fractional-order α is plotted according to the analytical result in Figure 8. The resonance is shown clearly in the fractional-order case. In other words, the fractional-order damping can induce a much stronger resonance than the ordinary linear damping. The corresponding two-dimensional plot is plotted in Figure 9. It also indicates the dependence of the resonance frequency and the magnitude of the resonance peak on the fractional-order α.

In Figures 10 and 11, the frequency response curve is given for the case $a > 0$ and $b < 0$. For this case, the original system has a double-hump potential. The resonance frequency and the resonance peak also depends on the fractional-order α.

From Figures 6−11, no matter the original system has the potential with different shapes, the resonance frequency and the resonance magnitude depends on the fractional-order α. The resonance frequency turns small with the increase of the value of α. The resonance magnitude turns large when the fractional-order moves away from $\alpha = 1$ gradually.

5 Conclusions

We investigate the dynamical behavior of a fractional Mathieu-Duffing oscillator which includes a fast parametric excitation and a slow external excitation. The linear stiffness coefficient in the system can induce a bifurcation
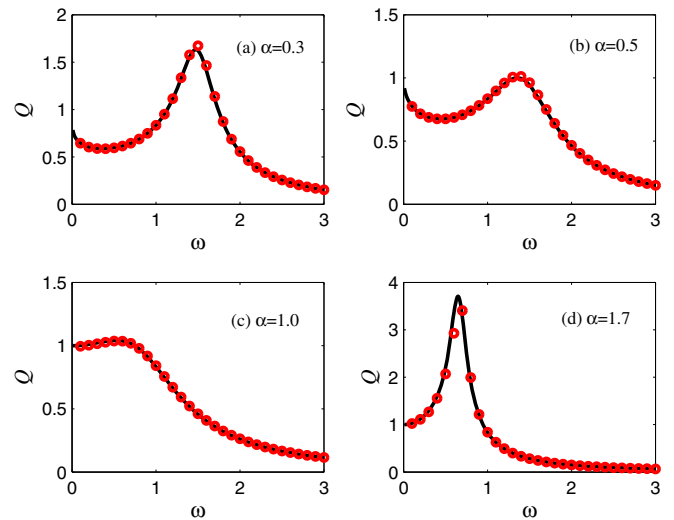

Fig. 9. The resonance frequency is shown for different values of the fractional-order α. The continuous lines are the analytical results and the discrete points are the numerical results. The simulation parameters are $\delta = 1.2$, $a = 1$, $b = 1$, $f = 0.1$, $F = 1$, $\Omega = 30$.
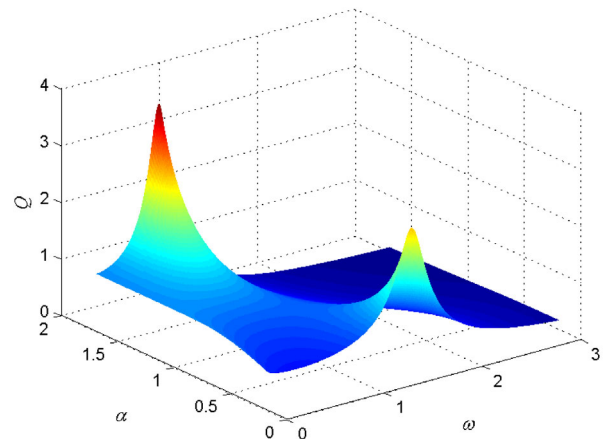

Fig. 10. The analytical result of the response amplitude Q versus the fractional-order α and the low-frequency ω. The simulation parameters are $\delta = 1.2$, $a = 1$, $b = -1$, $f = 0.1$, $F = 1$, $\Omega = 30$.

behavior. This type of bifurcation has been reported in some previous works. However, they did not give any numerical method to verify it. In this paper, a numerical method is given to verify the local bifurcation that is induced by the system parameter. Certainly, this method can also verify other types of local bifurcation that is induced by other parameters. Through this verification, we find that the constant components in the response just equals the equilibria of the equivalent system. Besides the constant component in the response, the resonance phenomenon is another focus in this paper. According to the nonlinear stiffness coefficient of the original system, the linear stiffness coefficient induced resonance appear with different patterns. If the nonlinear stiffness
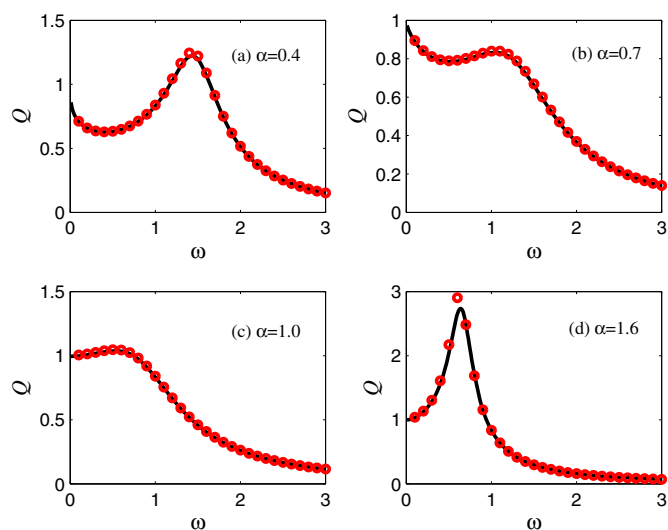
Fig. 11. The resonance frequency is shown for different values of the fractional-order α. The continuous lines are the analytical results and the discrete points are the numerical results. The simulation parameters are $\delta = 1.2$, $a = 1$, $b = -1$, $f = 0.1$, $F = 1$, $\Omega = 30$.

coefficient is positive, then the linear stiffness coefficient induced resonance may appear as a single-resonance or a double-resonance pattern. It depends on the value of the fractional-order. If the nonlinear stiffness coefficient is negative, the linear stiffness coefficient either cannot induce a resonance or it induces a single-resonance. It also depends on the value of the fractional-order closely. As to the resonance frequency, it decreases with the increase of the value of the fractional-order. Moreover, the resonance magnitude is larger when the damping is far away from the ordinary linear damping. In other words, the resonance is much stronger when the value of the fractional-order is far away from one. In a word, there are many more different dynamical properties in the fractional Mathieu-Duffing oscillator than that in the ordinary one. By investigating these new results, we might control a system effectively by choosing an appropriate system parameter or a fractional-order damping.

Author contribution statement

References

1. M. Ouni, N. Kahla, A. Preumont, Eng. Struct. **45**, 244 (2012)
2. H. Plat, I. Bucher, J. Sound Vib. **333**, 1408 (2014)
3. V. Kaajakari, A. Lal, Appl. Phys. Lett. **85**, 3923 (2009)
4. M.A. Mironov, P.A. Pyatakov, I.I. Konopatskaya, G.T. Clement, N.I. Vykhodtseva, Acoust. Phys. **55**, 567 (2009)
5. E.R. Rocio, G.R. David, H.R. Richard, J. Appl. Mech. **80**, 050903 (2013)
6. N.F. Pedersen, M.R. Samuelsen, K. Saermark, J. Appl. Phys. **44**, 5120 (2009)
7. M. Belhaq, S. Sah, Commun. Nonlin. Sci. Numer. Simul. **13**, 1706 (2008)
8. L. Mokni, M. Belhaq, F. Lakrad, Commun. Nonlin. Sci. Numer. Simul. **16**, 1720 (2011)
9. R.H. Huan, W.Q. Zhu, F. Ma, Z.H. Liu, Shock Vib. **2014**, 792673 (2014)
10. A. Fidlin, J.J. Thomsen, Int. J. Nonlin. Mech. **43**, 569 (2008)
11. J.J. Thomsen, J. Sound Vib. **311**, 1249 (2008)
12. B. Horton, J. Sieber, Int. J. Nonlin. Mech. **46**, 436 (2011)
13. R.J. Yatawara, R.D. Neilson, A.D.S. Barr, J. Sound Vib. **297**, 962 (2006)
14. P.S. Landa, P.V.E. McClintock, J. Phys. A **33**, L433 (2000)
15. V.N. Chizhevsky, G. Giacomelli, Phys. Rev. E **77**, 051126 (2008)
16. H. Yu, J. Wang, C. Liu, B. Deng, X. Wei, Chaos **21**, 043101 (2011)
17. A.A. Zaikin, L. López, J.P. Baltanás, J. Kurths, M.A.F. Sanjuán, Phys. Rev. E **66**, 011106 (2002)
18. S. Rajasekar, J. Used, Commun. Nonlin. Sci. Numer. Simul. **17**, 3435 (2012)
19. D.L. Hu, J.H. Yang, X.B. Liu, Comput. Biol. Med. **45**, 80 (2014)
20. M. Bordet, S. Morfu, Electron. Lett. **48**, 903 (2012)
21. F. Mainardi, G. Spada Creep, Eur. Phys. J. Special Topics **193**, 133 (2011)
22. D.C. Moutushi, C. Subrata, N. Soma, D. Shantanu, T. Sujata, Colloid Surface A **407**, 64 (2012)
23. F. Mainardi, *Fractional Calculus and Waves in Linear Viscoelasticity: An Introduction to Mathematical Models* (Imperial College Press, London, 2010)
24. K. Adolfsson, M. Enelund, P. Olsson, Mech. Time-Depend. Mat. **9**, 15 (2005)
25. V.E. Tarasov, Nonlin. Dyn. **71**, 663 (2013)
26. T.K. Ghosh, G. Baskaran, Phys. Rev. Lett. **87**, 186803 (2001)
27. N. Laskin, Phys. Rev. E **62**, 3135 (2000)
28. M. Klimek, Czech. J. Phys. **55**, 1447 (2005)
29. F. Riewe, Phys. Rev. E **55**, 3581 (1997)
30. C.T. Pedro, P. Ricardo, V.F. Nogueira, J. Electroanal. Chem. **560**, 25 (2003)
31. K.B. Oldham, Adv. Eng. Software **41**, 9 (2010)
32. B.J. West, J. Stat. Phys. **126**, 1285 (2007)
33. O.P. Agrawal, Nonlin. Dyn. **38**, 323 (2004)
34. J.H. Yang, H. Zhu, Chaos **22**, 013112 (2012)
35. J.H. Yang, H. Zhu, Commun. Nonlin. Sci. Numer. Simul. **18**, 1316 (2013)

36. J.H. Yang, M.A.F. Sánjuan, H.G. Liu, G. Cheng, J. Comput. Nonlin. Dyn. **10**, 061017 (2015)
37. J.H. Yang, M.A.F. Sánjuan, F. Tian, H.F. Yang, Int. J. Bifurcat. Chaos **25**, 1550023 (2015)
38. C.A. Monje, Y. Chen, B.M. Vinagre, D. Xue, V. Feliu, *Fractional- Order Systems and Controls* (Springer, London, 2010)
39. J.J. Thomsen, *Vibrations and Stability: Advanced Theory, Analysis, and Tools* (Springer-Verlag, Berlin, Heidelberg, 2003)
40. I.I. Blekhman, *Selected Topics in Vibrational Mechanics* (World Scientific, Singapore, 2003)
41. I.I. Blekhman, P.S. Landa, Int. J. Nonlin. Mech. **39**, 421 (2004)
42. S. Jeyakumari, V. Chinnathambi, S. Rajasekar, M.A.F. Sanjuán, Phys. Rev. E **80**, 046608 (2009)
43. S. Jeyakumari, V. Chinnathambi, S. Rajasekar, M.A.F. Sanjuán, Chaos **19**, 043128 (2009)
44. T.L.M. Djomo Mbong, M. Siewe Siewe, C. Tchawoua, Commun. Nonlin. Sci. Numer. Simul. **22**, 228 (2015)
45. S. Hu, W. Chen, X.F. Gou, Adv. Vib. Eng. **10**, 187 (2011)
46. Z.J. Fu, W. Chen, H.T. Yang, J. Comput. Phys. **235**, 52 (2013)
47. G.F. Pang, W. Chen, Z.J. Fu, J. Comput. Phys. **293**, 280 (2015)
48. W. Deng, J. Comput. Phys. **227**, 1510 (2007)
49. C. Li, F. Zeng, *Numerical Methods for Fractional Calculus* (Chapman and Hall, New York, 2015)
50. J. Cao, C. Ma, H. Xie, Z. Jiang, J. Comput. Nonlin. Dyn. **5**, 041012 (2010)